Nano Research

ISSN 1998-0124 CN 11-5974/O4
https://doi.org/10.1007/s12274-022-4315-5

Research Article

Strain engineering of anisotropic light–matter interactions in one-dimensional P–P chain of SiP_2

HPSTAR 1438-2022

Fanghua Cheng[1,§], Junwei Huang[1,§], Feng Qin[1,§], Ling Zhou[1], Xueting Dai[1], Xiangyu Bi[1], Caorong Zhang[1], Zeya Li[1], Ming Tang[1], Caiyu Qiu[1], Yangfan Lu[2], Huiyang Gou[3], and Hongtao Yuan[1] (✉)

[1] *National Laboratory of Solid State Microstructures and Jiangsu Key Laboratory of Artificial Functional Materials, College of Engineering and Applied Sciences, Nanjing University, Nanjing 210000, China*
[2] *College of Materials Science and Engineering, National Engineering Research Center for Magnesium Alloys, Chongqing University, Chongqing 400030, China*
[3] *Center for High Pressure Science and Technology Advanced Research, Beijing 100094, China*
[§] *Fanghua Cheng, Junwei Huang, and Feng Qin contributed equally to this work.*

Received: 19 November 2021 / **Revised:** 28 January 2022 / **Accepted:** 11 March 2022

ABSTRACT

Strain engineering can serve as a powerful technique for modulating the exotic properties arising from the atomic structure of materials. Examples have been demonstrated that one-dimensional (1D) structure can serve as a great platform for modulating electronic band structure and phonon dispersion via strain control. Particularly, in a van der Waals material silicon diphosphide (SiP_2), quasi-1D zigzag phosphorus–phosphorus (P–P) chains are embedded inside the crystal structure, and can show unique phonon vibration modes and realize quasi-1D excitons. Manipulating those optical properties by the atom displacements via strain engineering is of great interest in understanding underlying mechanism of such P–P chains, however, which remains elusive. Herein, we demonstrate the strain engineering of Raman and photoluminescence (PL) spectra in quasi-1D P–P chains and resulting in anisotropic manipulation in SiP_2. We find that the phonon frequencies of SiP_2 in Raman spectra linearly evolve with a uniaxial strain along/perpendicular to the quasi-1D P–P chain directions. Interestingly, by applying tensile strain along the P–P chains, the band gap energy of strained SiP_2 can significantly decrease with a tunable value of ~ 55 meV. Based on arsenic (As) element doping into SiP_2, the strain-induced redshifts of phonon frequencies decrease, indicating the stiffening of the phonon vibration with the increased arsenic doping level. Such results provide an opportunity for strain engineering of the light–matter interactions in the quasi-1D P–P chains of SiP_2 crystal for potential optical applications.

KEYWORDS

strain engineering, silicon diphosphide, Raman, photoluminescence

1 Introduction

Anisotropic crystal structures and reduced crystal symmetry of materials play key roles in determining their electronic and optical properties [1–6]. Examples of anisotropic crystal structures have been found in layered two-dimensional (2D) materials such as black phosphorus (BP) [7], ReS_2 [8], TiS_3 [9], and ZrS_3 [10]. Unlike materials with high symmetry showing isotropic physical properties, many 2D materials with reduced crystal symmetry display strong in-plane anisotropic properties. Such an anisotropic crystal structure results in an apparently distinct response when applying strain along different crystalline orientations [11]. Uniaxial mechanical strain can usually serve as a powerful way to modulate light–matter interactions by manipulating the crystal structure and thus is of great interest and significance in practical applications such as strain sensors and polarization-sensitive detectors [12–15]. Among a variety of material candidates, van der Waals 2D materials are particularly suitable for local strain engineering due to their atomically thin thickness and great flexibility [16–19]. Therefore, it is highly desirable to study the strain engineering of Raman and photoluminescence (PL) characteristics for phonon vibration modes and excitonic states in anisotropic 2D materials [20–23].

Herein, combined with optical measurements of the Raman and PL spectra, we demonstrate that strain engineering can effectively manipulate the phonon frequencies as well as the band gap energy in anisotropic layered SiP_2. The phonon frequencies of SiP_2 decrease gradually and linearly with applying uniaxial tensile strain along the phosphorus–phosphorus (P–P) chain direction in the SiP_2 crystal, while those frequencies increase with uniaxial tensile strain applied perpendicularly. Interestingly, we find that the phonon vibration becomes stiff when arsenic (As) is intentionally doped into SiP_2, and thus, the atomic bonding strength between atoms in the crystal is increased. Note that in the PL spectra of wrinkled flakes, the strain can induce redshifts of the peak in the PL spectra, and the decreased values in the optical band gap of SiP_2 can be as significant as ~ 55 meV, indicating that strain engineering can produce large deformations of the lattice structure related to the P–P chains and lead to the evolution of the energy band structure in layered SiP_2. Such results support the view that strain engineering can serve as an enabling tool to

Address correspondence to htyuan@nju.edu.cn

explore novel physics originating from the zigzag P–P chains in SiP_2, providing an effective method to manipulate the atomic structure and tune the specific optical properties of 2D materials for potential optical applications.

2 Experiments

We intentionally chose in-plane anisotropic SiP_2 to study strain engineering for tuning the Raman and PL properties for the following reasons. First, the atomic structure of SiP_2 has an orthorhombic structure with in-plane lattice constants a = 10.091 Å and b = 3.439 Å (space group No. 62, *Pnma*) [24–26], providing strong in-plane anisotropy, as schematically shown in Fig. 1(a). Second, SiP_2 contains two kinds of inequivalent phosphorus atomic sites distinguished by their bonding surroundings. For the P atom bonding to one Si atom and two other P atoms, those neighboring P atoms bond together, forming embedded quasi-one-dimensional (quasi-1D) zigzag P–P chains along the y direction. Note that such zigzag P–P chains can generate highly anisotropic phonon vibrations and PL properties in SiP_2, which will be one of the main focuses of this study. Third, an exotic excitonic state with strong anisotropy originates from the unique quasi-1D electronic state along the zigzag P–P chains in SiP_2. Therein, emergent many-body phenomena are related to the exciton–phonon interaction. Therefore, in-plane anisotropic SiP_2 can serve as a unique material platform to investigate the phonon vibration modes and excitonic states via strain engineering.

Two methods were used to apply strain for the Raman and PL measurements. On the one hand, as shown in Fig. 1(a), polyethylene terephthalate (PET) was used as a flexible substrate for applying tensile strain on few-layer SiP_2 for strain-dependent Raman spectra measurements. The SiP_2 flakes were mechanically exfoliated with polydimethylsiloxane (PDMS) and directly transferred onto the surface of a flexible PET substrate [27], which was processed inside a glove box (protected with 99.99% purity N_2) to prevent the sample from oxidizing. To identify the direction of applied strain, we found that the exfoliated SiP_2 flake had a rectangular shape in which the long and short edges corresponded to the y and x directions (more details are shown in Figs. S1 and S2 in the Electronic Supplementary Material (ESM)). On the other hand, for strain-dependent PL spectra measurements, a wrinkled flake was intentionally generated by transferring the sample onto i) pre-stretched PDMS or ii) Si/SiO_2 substrate with pre-patterned SiO_2 nanowires. Atomic force microscopy (AFM) was used to identify the thickness of the samples and the shape of the wrinkled structure. In optical measurements, both Raman and PL spectra were obtained by the WITec Alpha 300 system at room temperature using a ×50 objective lens. The laser had a wavelength of 532 nm and power of 1 mW. The integrated time was 20 seconds and was repeated 5 times. All optical measurements were performed under the protection of a N_2 atmosphere (99.99% purity). Normally, the uniaxial tensile strain value ε applied on the sample can be estimated by $\varepsilon \sim \Delta L/L_0$, where L_0 is the initial length of a SiP_2 flake before applying strain, and ΔL is the increased length of the sample after stretching. The values of L_0 and ΔL can be obtained from the optical images of the strained SiP_2 flake, and the measurement method and results are shown in Figs. S1–S3 in the ESM.

3 Results and discussion

3.1 Raman spectra of SiP_2 under uniaxial tensile strain

To detect the strain response of the vibration modes in layered SiP_2 thin flakes, we performed Raman measurements based on a homemade mechanical strain stage with PET as a flexible supporting substrate (shown in Fig. S4 in the ESM). With this stage, we can precisely control the magnitude of uniaxial tensile strain applied along the y and x directions in SiP_2, as shown in Fig. 1(b). Note that the strain is uniformly distributed in the entire SiP_2 flake, which is confirmed by the Raman mapping image in Fig. S4(c) in the ESM. Since the lattice symmetry does not change during stretching (shown in Fig. S5 in the ESM), applied strain can only cause the shift of the Raman peaks without symmetry-

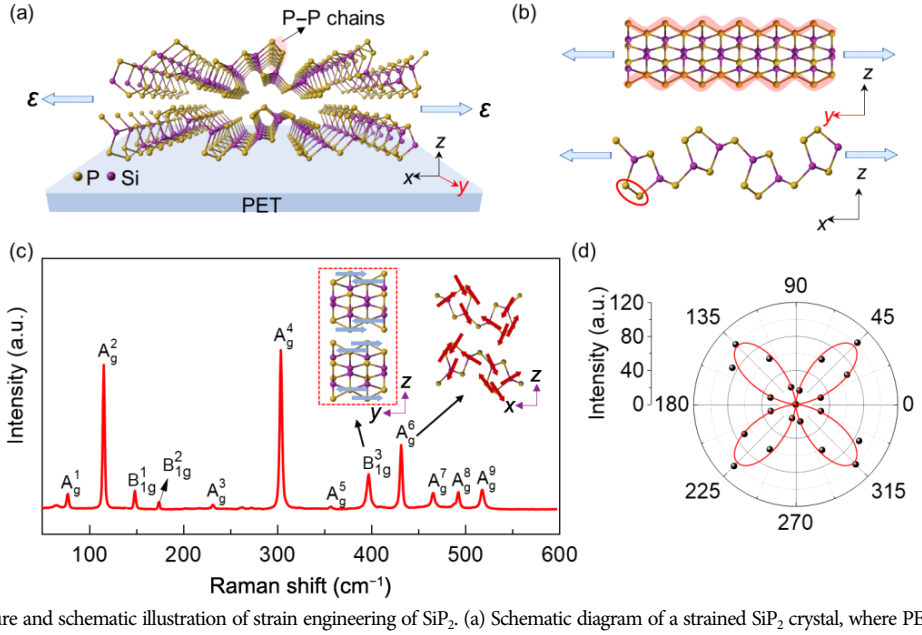

Figure 1 Crystal structure and schematic illustration of strain engineering of SiP_2. (a) Schematic diagram of a strained SiP_2 crystal, where PET is selected as a flexible substrate. Si and P atoms are represented by purple and yellow spheres, respectively. The *xyz* coordinate system is defined based on the crystal structure, as shown in the lower right corner. The quasi-1D zigzag P–P chains are embedded along the y direction (highlighted by pink shadow). Blue arrows display the direction of tension when applying strain. (b) Uniaxial strain applied along two perpendicular directions of the SiP_2 crystal. The upper (or lower) panel shows stretching along the y (or x) direction, and the P–P chains are highlighted. (c) Raman spectrum of a SiP_2 thin flake excited by a 532-nm laser. The characteristic vibration modes are labeled. The inset shows the vibration modes of B_{1g}^3 (left panel) and A_g^6 (right panel). (d) Polar plot of the Raman peak intensity of the B_{1g}^3 mode from polarized Raman spectra, which indicates the fourfold symmetry of Raman scattering tensor elements.

breaking-induced splitting, which provides an advantage to study the anisotropic Raman spectra under strain. Figure 1(c) shows the Raman spectrum of a few-layer pristine SiP_2 with no strain. Twelve Raman peaks are labeled as A_g^1 (77 cm^{-1}), A_g^2 (116 cm^{-1}), B_{1g}^1 (149 cm^{-1}), B_{1g}^2 (174 cm^{-1}), A_g^3 (232 cm^{-1}), A_g^4 (304 cm^{-1}), A_g^5 (358 cm^{-1}), B_{1g}^3 (398 cm^{-1}), A_g^6 (433 cm^{-1}), A_g^7 (467 cm^{-1}), A_g^8 (494 cm^{-1}), and A_g^9 (519 cm^{-1}), are consistent with previous Raman studies on SiP_2 [28]. The B_{1g}^3 Raman peak reflects the characteristic vibration modes of the P–P chains, as schematically represented in the inset of Fig. 1(c) and Fig. S6 in the ESM. From the polarized Raman spectra shown in Fig. 1(d), one can see that the B_{1g}^3 mode related to the P–P chains in SiP_2 shows fourfold rotational symmetry. In this study, we will mainly investigate B_{1g}^3 and A_g^6 vibration modes, which are the most sensitive to the applied strain in our experiments.

Figure 2(a) shows the evolution of the Raman spectra of few-layer SiP_2 with increased strain from 0% to 1.07% along the y direction. One can see in Figs. 2(b) and 2(c) that both B_{1g}^3 and A_g^6 peaks shift to lower wavenumbers with increased strain. The B_{1g}^3 peak shows a more obvious redshift than the A_g^6 peak, suggesting that the former is more sensitive to strain than the latter. To describe this sensitivity quantitatively, we calculate the average slope Δ (cm^{-1}/%), which is obtained from the linear fit to the Raman shift data as a function of applied strain. Thus, the Δ_x and Δ_y values represent the strain response of the strain along the x and y directions of SiP_2, respectively. Along the y direction, when ε is up to 1.07%, the B_{1g}^3 peak shows a redshift with Δ_y = −7.06 cm^{-1}/%, and the A_g^6 peak shows a redshift with Δ_y = −4.81 cm^{-1}/%. In contrast, in Figs. 2(d)–2(f), when ε along the x direction is increased from 0% to 4.65%, both B_{1g}^3 and A_g^6 peaks show blueshifts. The Δ_x values of B_{1g}^3 and A_g^6 peaks are approximately 2.05 cm^{-1}/% and 0.90 cm^{-1}/%, respectively. One can see that the Δ_y values are significantly greater than the Δ_x values, indicating that SiP_2 is a highly anisotropic material and shows a higher strain-dependent sensitivity along the P–P chains. The intensity of both B_{1g}^3 and A_g^6 peaks decreases with increasing strain in the y and x directions (shown in Fig. S7 in the ESM).

To further understand the microscopic atomic displacements of strained SiP_2, we calculated Poisson's ratio σ (defined as $-\Delta_x/\Delta_y$) for B_{1g}^3 and A_g^6 Raman modes, which are sensitive to atomic bonding strength. From Figs. 2(c) and 2(f), the σ value for the A_g^6 mode is estimated to be approximately 0.19, consistent with the value of 0.16 obtained from the optical microscopy image (shown in Table S1 and Fig. S8 in the ESM). SiP_2 has a greater Poisson's ratio than MoS_2 (σ = 0.125) [29], indicating the strong strain-dependent anisotropy of SiP_2. In contrast, from Figs. 2(b) and 2(e), Poisson's ratio for the B_{1g}^3 Raman mode is estimated to be approximately 0.29. The significant difference in the Poisson's ratio of B_{1g}^3 and A_g^6 Raman modes can be attributed to the following reason. The atomic vibration of the B_{1g}^3 mode only involves those P atoms within the P–P chains. Due to the particular atomic structure of SiP_2, the uniaxial tensile strain along the x direction (perpendicular to the P–P chains) can cause larger position displacements of those P atoms within the P–P chains than that of Si atoms and the remaining P atoms. In contrast, the atomic displacements of all atoms under strain along the y direction are similar. Therefore, the uniaxial tensile strain along the x direction contributes to a larger shift of the B_{1g}^3 peak and leads to an overestimation of Poisson's ratio.

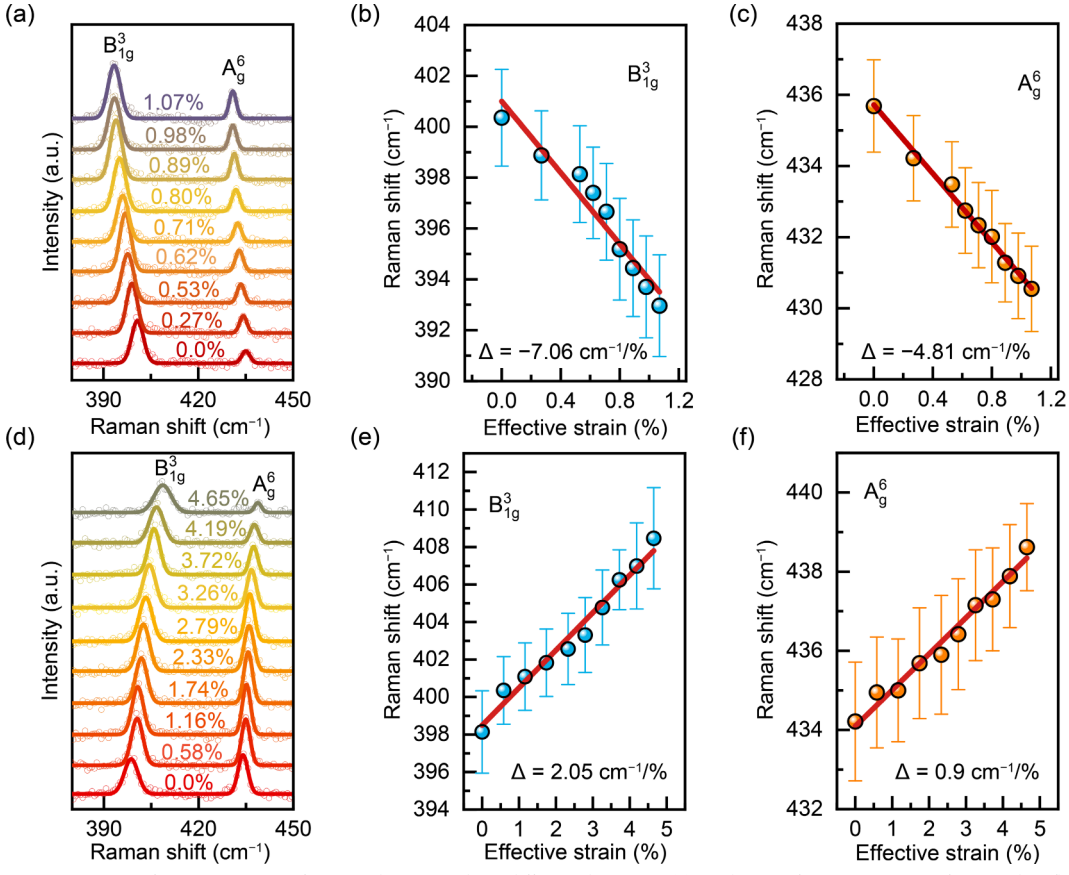

Figure 2 Anisotropic response of Raman spectra of SiP_2 under strain along different directions. (a) Evolution of Raman spectra of a SiP_2 thin flake under strain applied along the y direction. With increased strain up to 1.07%, both B_{1g}^3 and A_g^6 modes show redshifts. (b) and (c) Evolution of Raman shifts of both B_{1g}^3 and A_g^6 modes under strain along the y direction. Both B_{1g}^3 and A_g^6 modes show linear redshifts whose values depend on tensile strain along the y direction. (d) Evolution of Raman spectra of a SiP_2 thin flake under strain applied along the x direction. With increased strain up to 4.65%, both B_{1g}^3 and A_g^6 modes show blueshifts. (e) and (f) Evolution of Raman shifts of both B_{1g}^3 and A_g^6 modes under strain along the x direction. Both B_{1g}^3 and A_g^6 modes show linear blueshifts whose values depend on tensile strain along the x direction.

3.2 Effect of arsenic (As) substitution on Raman spectra

To verify the relations between the strong strain-dependent anisotropy and the quasi-1D P–P chains of SiP_2, we further investigated the Raman spectra by intentionally doping the arsenic atoms, as schematically shown in Fig. 3(a). We synthesized a series of doped SiP_2 with different stoichiometric arsenic concentrations of 0%, 10%, 20%, 30%, 40%, and 60%, as shown in Fig. S9 in the ESM.

Figure 3(b) shows the evolution of the Raman spectra of SiP_2-As10 (nominal As doping level of 10%) under strain applied from 0% to 2.6% along the y direction. Similar to pristine SiP_2, both B_{1g}^3 and A_g^6 modes shift toward lower wavenumbers. The evolution of the B_{1g}^3 mode in our strained samples with different doping levels is shown in Fig. 3(c). Three important points should be addressed here. First, the B_{1g}^3 mode at zero strain shows a blueshift with increased arsenic doping, showing a specific substitution of arsenic for P atoms in the SiP_2 crystal and remaining for further study. Second, when the strain gradually increases, the B_{1g}^3 modes of all samples show redshifts. This implies a similar strain-dependent evolution along the y direction for all arsenic-doped SiP_2 flakes. Third, the average slope Δ for the B_{1g}^3 mode significantly decreases with increasing arsenic doping level, as shown in Fig. 3(d). These results indicate that heavy arsenic atoms increase the bonding strength and further reduce the strain-dependent sensitivity and confirm that the quasi-1D P–P chains are directly related to the strong strain-dependent anisotropy of SiP_2.

3.3 PL spectra of strained SiP_2 with a wrinkled structure

To understand the evolution of the band gap associated with the P–P chains, which is the source of the conduction-band electron wave function, we performed PL measurements in strained SiP_2 flakes. The PET substrate generally shows a large PL background overlapping with the PL signals of SiP_2, which will cause technical difficulties for studying PL properties. Herein, we performed measurements for strain-engineered PL spectra by using an alternative method with a clean background (shown in Fig. S10 in the ESM), as described in the Experimental Section. As shown in Fig. 4(a), the local uniaxial strain is obtained by intentionally wrinkling a SiP_2 flake to form a bending structure on a pre-stretched flexible substrate, which has been widely used to produce strain with multiple wrinkles in layered materials [29]. The bottom panel of Fig. 4(a) shows the AFM image of an example of the wrinkle in a strained SiP_2 flake. The strain ε at the top of the wrinkle can be estimated as $\varepsilon \sim \pi^2 h\delta/(1-\sigma^2)\lambda^2$, where σ is Poisson's ratio of SiP_2, h is the thickness of the flake, and δ and λ are the height and width of the wrinkle, respectively [29]. These values can be obtained from the wrinkle geometry, as shown in the top panel of Fig. 4(b), and more details are shown in Fig. S11 in the ESM.

To understand the strain distribution around the wrinkle, we conducted a line scan for the PL measurements across the wrinkle, and the results are shown in Fig. 4(c). Note that the PL spectra show redshifts from the flat bottom to the top of the bent wrinkle. This indicates that strain reduces the band gap of SiP_2. The largest redshift of the PL spectra is observed on the top of the wrinkle, indicating that the maximum strain is achieved there, similar to a previous report on MoS_2 [29]. The evolution of the band gap energy with location is shown in the bottom panel of Fig. 4(b). The PL spectra obtained at the top of the wrinkle have a maximum redshift as high as 55 meV under a strain of 1.88% compared to that in the flat area, which indicates that the applied strain reduces the band gap. According to the above strain estimation, the maximum strains generated at the top of the three wrinkles in the same SiP_2 flake are 1.34%, 1.53%, and 1.88%, and the corresponding PL spectra are shown in Fig. 4(d). Figure 4(e) shows the evolution of the band gap with strain caused by wrinkles. With increased effective strain, the band gap energy decreases. The band gap of SiP_2 is modulated by strain with a modulation efficiency of 26 meV/% and displays a gradual redshift from the bottom to the top of the wrinkle at different angles from the P–P chain (shown in Fig. S12 in the ESM). Strain can only reduce the band gap energy of SiP_2 without causing symmetry breaking (shown in Fig. S13 in the ESM). These observations shed light on understanding the microscopic excitonic properties arising from the quasi-1D P–P chains in SiP_2.

4 Conclusions

In summary, we demonstrate strain engineering on anisotropic light–matter interactions in quasi-1D P–P chains of layered SiP_2. We find that the lattice structure and phonon vibration of SiP_2 can be manipulated with uniaxial strain, providing a unique means to design and control the light–matter interactions for atomically thin SiP_2-based devices. As the arsenic doping level increases, the absolute values of the slopes of the strain-dependent phonon energies decrease in the arsenic-doped SiP_2 samples. With PL measurements of the wrinkled SiP_2 samples, the PL peak shows a redshift, and the band gap energy decreases with increasing strain.

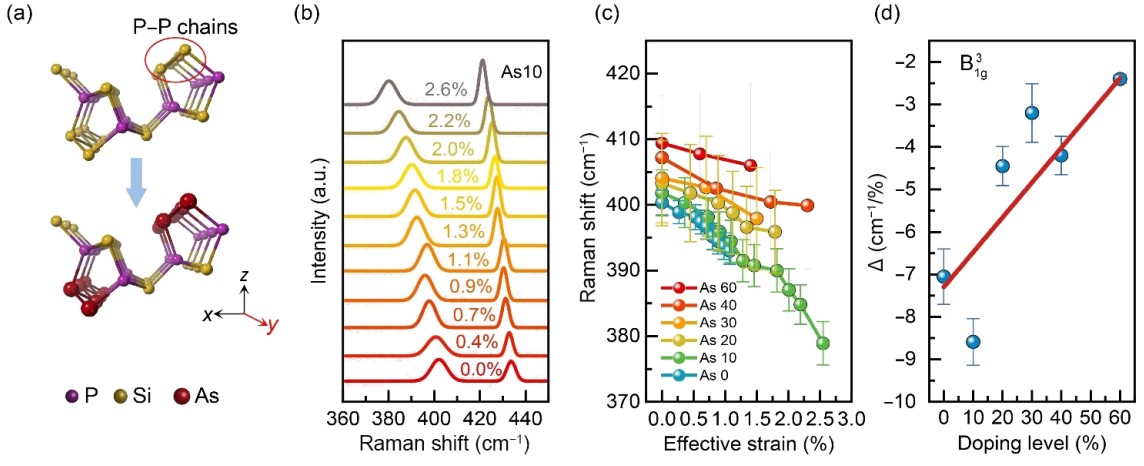

Figure 3 Raman spectra of As-doped SiP_2 under strain along the y direction. (a) Schematic depiction of substitution of the P atoms within the P–P chains by As atoms. (b) Evolution of Raman spectra of SiP_2-As10 (nominal As doping level of 10%) under tensile strain applied from 0% to 2.6% along the y direction. (c) Evolution of the strained B_{1g}^3 Raman peak of doped SiP_2 with different As concentrations of 0%, 10%, 20%, 30%, 40%, and 60%. (d) The average slope Δ for the B_{1g}^3 modes as a function of doping level.

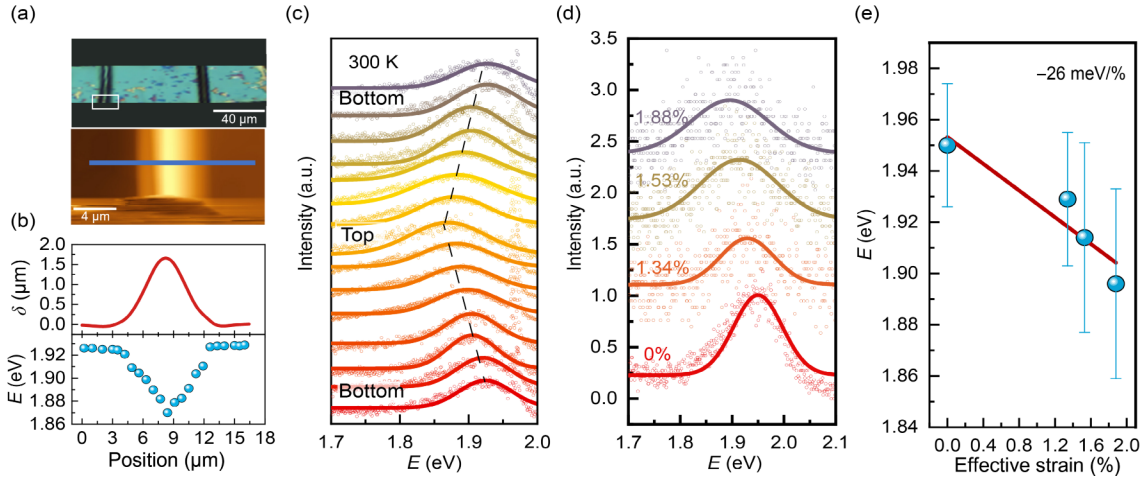

Figure 4 Photoluminescence of a strain-engineered wrinkled SiP_2 thin flake. (a) Optical image of a SiP_2 thin flake with a wrinkled structure (top panel) and AFM topography image of the area marked by a white rectangle (bottom panel). (b) Height profile (top panel) along the blue line crossing the wrinkle shown in the AFM image in (a). Based on the shape of the wrinkle, the induced tensile strain along the *y* direction on the top of the wrinkle can be estimated. The bottom panel shows the energy of the optical band gap at different positions along the blue line in (a). The energy of the optical band gap displays the largest redshift at the top of the wrinkle, where the largest tensile strain is induced. (c) The PL spectra measured along the blue line crossing the wrinkle. The hollow circles represent the original data, and the solid curves are obtained by Gaussian fitting. The black dashed line guides the evolution of the energy of the optical band gap, which displays a gradual redshift when the laser spot moves from the bottom to the top of the wrinkle. (d) PL spectra measured on the tops of three different wrinkles. The hollow circles represent the experimental data of the PL spectra, and the solid curves are obtained by Gaussian fitting. (e) Strain dependence of the energy of the optical band gap obtained from the Gaussian fittings in (d). A band gap modulation ΔE as large as ~ 55 meV is observed in a SiP_2 thin flake strained up to 1.88% along the *y* direction, with a modulation efficiency of 26 meV/%.

These observations suggest strain engineering as a powerful route to explore novel physics in anisotropic materials, opening additional opportunities for potential optics and optoelectronics applications.

Acknowledgements

This research was supported by the National Natural Science Foundation of China (Nos. 51861145201, 52072168, 21733001, and 91750101), the National Key Basic Research Program of the Ministry of Science and Technology of China (Nos. 2018YFA0306200 and 2021YFA1202901), and Jiangsu Key Laboratory of Artificial Functional Materials. L. Y. F. acknowledges financial support from the start-up fund of Chongqing University (No. 02110011044171).

Electronic Supplementary Material: Supplementary Material ((1) measurement of sample length with applied strain in the *y* and *x* directions, (2) measurement method of sample length with applied strain, (3) details of the strain application procedure, (4) polarized Raman spectra of the B_{1g}^3 mode under strain, (5) lattice vibrations with fourfold degeneracy of the B_{1g}^3 mode, (6) peak intensity analysis of Raman spectra of SiP_2 under uniaxial tensile strain, (7) Measurement results of Poisson's ratio value, (8) Raman spectra of $SiP_{2-x}As_x$ alloys under strain, (9) optical background of stretchable substrates, (10) strain analysis in the SiP_2 wrinkling structure, (11) PL spectra of the SiP_2 wrinkling structure along different crystal directions, and (12) polarized PL spectra under strain) is available in the online version of this article at https://doi.org/10.1007/s12274-022-4315-5.

References

[1] Cao, Y.; Fatemi, V.; Fang, S. A.; Watanabe, K.; Taniguchi, T.; Kaxiras, E.; Jarillo-Herrero, P. Unconventional superconductivity in magic-angle graphene superlattices. *Nature* **2018**, *556*, 43–50.

[2] Khang, D. Y.; Jiang, H. Q.; Huang, Y. N.; Rogers, J. A. A stretchable form of single-crystal silicon for high-performance electronics on rubber substrates. *Science* **2006**, *311*, 208–212.

[3] Wu, W. Z.; Wang, L.; Li, Y. L.; Zhang, F.; Lin, L.; Niu, S. M.; Chenet, D.; Zhang, X.; Hao, Y. F.; Heinz, T. F. et al. Piezoelectricity of single-atomic-layer MoS_2 for energy conversion and piezotronics. *Nature* **2014**, *514*, 470–474.

[4] Khang, D. Y.; Rogers, J. A.; Lee, H. H. Mechanical buckling: Mechanics, metrology, and stretchable electronics. *Adv. Funct. Mater.* **2009**, *19*, 1526–1536.

[5] Koo, W. H.; Jeong, S. M.; Araoka, F.; Ishikawa, K.; Nishimura, S.; Toyooka, T.; Takezoe, H. Light extraction from organic light-emitting diodes enhanced by spontaneously formed buckles. *Nat. Photon.* **2010**, *4*, 222–226.

[6] Wang, M. C.; Leem, J.; Kang, P.; Choi, J.; Knapp, P.; Yong, K. O. N.; Nam, S. Mechanical instability driven self-assembly and architecturing of 2D materials. *2D Mater.* **2017**, *4*, 022002.

[7] Roldán, R.; Castellanos-Gomez, A.; Cappelluti, E.; Guinea, F. Strain engineering in semiconducting two-dimensional crystals. *J. Phys. Condens. Matter* **2015**, *27*, 313201.

[8] An, C. H.; Xu, Z. H.; Shen, W. F.; Zhang, R. J.; Sun, Z. Y.; Tang, S. J.; Xiao, Y. F.; Zhang, D. H.; Sun, D.; Hu, X. D. et al. The opposite anisotropic piezoresistive effect of ReS_2. *ACS Nano* **2019**, *13*, 3310–3319.

[9] Island, J. O.; Barawi, M.; Biele, R.; Almazán, A.; Clamagirand, J. M.; Ares, J. R.; Sánchez, C.; Van Der Zant, H. S. J.; Álvarez, J. V.; D'Agosta, R. et al. TiS_3 transistors with tailored morphology and electrical properties. *Adv. Mater.* **2015**, *27*, 2595–2601.

[10] Xie, J. F.; Wang, R. X.; Bao, J.; Zhang, X. D.; Zhang, H.; Li, S.; Xie, Y. Zirconium trisulfide ultrathin nanosheets as efficient catalysts for water oxidation in both alkaline and neutral solutions. *Inorg. Chem. Front.* **2014**, *1*, 751–756.

[11] Ling, X.; Huang, S. X.; Hasdeo, E. H.; Liang, L. B.; Parkin, W. M.; Tatsumi, Y.; Nugraha, A. R. T.; Puretzky, A. A.; Das, P. M.; Sumpter, B. G. et al. Anisotropic electron–photon and electron–phonon interactions in black phosphorus. *Nano Lett.* **2016**, *16*, 2260–2267.

[12] Jain, J. R.; Hryciw, A.; Baer, T. M.; Miller, D. A. B.; Brongersma, M. L.; Howe, R. T. A micromachining-based technology for enhancing germanium light emission via tensile strain. *Nat. Photon.* **2012**, *6*, 398–405.

[13] Feng, J.; Qian, X. F.; Huang, C. W.; Li, J. Strain-engineered artificial atom as a broad-spectrum solar energy funnel. *Nat. Photon.* **2012**, *6*, 866–872.

[14] Yuan, H. T.; Liu, X. G.; Afshinmanesh, F.; Li, W.; Xu, G.; Sun, J.; Lian, B.; Curto, A. G.; Ye, G. J.; Hikita, Y. et al. Polarization-

sensitive broadband photodetector using a black phosphorus vertical p-n junction. *Nat. Nanotechnol.* **2015**, *10*, 707–713.
[15] Guo, Q. S.; Pospischil, A.; Bhuiyan, M.; Jiang, H.; Tian, H.; Farmer, D.; Deng, B. C.; Li, C.; Han, S. J.; Wang, H. et al. Black phosphorus mid-infrared photodetectors with high gain. *Nano Lett.* **2016**, *16*, 4648–4655.
[16] Polyzos, I.; Bianchi, M.; Rizzi, L.; Koukaras, E. N.; Parthenios, J.; Papagelis, K.; Sordan, R.; Galiotis, C. Suspended monolayer graphene under true uniaxial deformation. *Nanoscale* **2015**, *7*, 13033–13042.
[17] Lee, C.; Wei, X. D.; Kysar, J. W.; Hone, J. Measurement of the elastic properties and intrinsic strength of monolayer graphene. *Science* **2008**, *321*, 385–388.
[18] Bertolazzi, S.; Brivio, J.; Kis, A. Stretching and breaking of ultrathin MoS_2. *ACS Nano* **2011**, *5*, 9703–9709.
[19] Cooper, R. C.; Lee, C.; Marianetti, C. A.; Wei, X. D.; Hone, J.; Kysar, J. W. Nonlinear elastic behavior of two-dimensional molybdenum disulfide. *Phys. Rev. B* **2013**, *87*, 035423.
[20] Yun, W. S.; Han, S. W.; Hong, S. C.; Kim, I. G.; Lee, J. D. Thickness and strain effects on electronic structures of transition metal dichalcogenides: 2H-MX_2 semiconductors (M = Mo, W; X = S, Se, Te). *Phys. Rev. B* **2012**, *85*, 033305.
[21] Ghorbani-Asl, M.; Borini, S.; Kuc, A.; Heine, T. Strain-dependent modulation of conductivity in single-layer transition-metal dichalcogenides. *Phys. Rev. B* **2013**, *87*, 235434.
[22] Miró, P.; Ghorbani-Asl, M.; Heine, T. Spontaneous ripple formation in MoS_2 monolayers: Electronic structure and transport effects. *Adv. Mater.* **2013**, *25*, 5473–5475.
[23] Molina-Sánchez, A.; Sangalli, D.; Hummer, K.; Marini, A.; Wirtz, L. Effect of spin–orbit interaction on the optical spectra of single-layer, double-layer, and bulk MoS_2. *Phys. Rev. B* **2013**, *88*, 045412.
[24] Wadsten, T. The crystal structures of SiP_2, $SiAs_2$, and GeP. *Acta Chem. Scand.* **1967**, *21*, 593–594.
[25] Novoselov, K. S.; Jiang, D.; Schedin, F.; Booth, T. J.; Khotkevich, V. V.; Morozov, S. V.; Geim, A. K. Two-dimensional atomic crystals. *Proc. Natl. Acad. Sci. USA* **2005**, *102*, 10451–10453.
[26] Zhang, X.; Wang, S. P.; Ruan, H. P.; Zhang, G. D.; Tao, X. T. Structure and growth of single crystal SiP_2 using flux method. *Solid State Sci.* **2014**, *37*, 1–5.
[27] Vella, D.; Bico, J.; Boudaoud, A.; Roman, B.; Reis, P. M. The macroscopic delamination of thin films from elastic substrates. *Proc. Natl. Acad. Sci. USA* **2009**, *106*, 10901–10906.
[28] Meier, M.; Weihrich, R. *Ab initio* simulation of the fundamental vibrational frequencies of selected pyrite-type pnictides. *Chem. Phys. Lett.* **2008**, *461*, 38–41.
[29] Castellanos-Gomez, A.; Roldán, R.; Cappelluti, E.; Buscema, M.; Guinea, F.; Van Der Zant, H. S. J.; Steele, G. A. Local strain engineering in atomically thin MoS_2. *Nano Lett.* **2013**, *13*, 5361–5366.